RSC Pharmaceutics

ROYAL SOCIETY OF CHEMISTRY

PAPER

View Article Online
View Journal | View Issue

Cite this: *RSC Pharm.*, 2025, **2**, 1139

Systematic screening of excipients to stabilize aerosolized lipid nanoparticles for enhanced mRNA delivery†

Brittany J. Heiser, [a] Mae M. Lewis, [a] Meysam Mohammadi Zerankeshi, [b] Emily K. Netemeyer, [a] Ashlee M. Hernandez, [a] Alexander E. Marras [a,b] and Debadyuti Ghosh *[c]

Aerosolized lipid nanoparticles (LNPs) delivering mRNA are an attractive strategy for use in local, inhalable therapy to treat patients with lung diseases. However, a major barrier to delivering aerosolized mRNA LNPs is the shear forces encountered during aerosolization. These forces lead to significant morphology changes and subsequent decrease in efficacy of mRNA delivery. To best retain the physicochemical properties of mRNA LNPs during aerosolization, we took a formulation-based strategy to stabilize LNPs. We used a design-of-experiment (DOE) approach to comprehensively screen rationally chosen excipients at multiple concentrations. Excipients were carefully selected based on their use in clinically approved inhaled products or their ability to support lipid membrane properties. These excipients were added to the same mRNA LNP composition after formulation, were subsequently characterized, and used to transfect human lung cells at air–liquid interface. From this systematic screen, we identified that the addition of our lead candidate, poloxamer 188, best stabilizes LNP size throughout aerosolization and enhances mRNA expression after aerosolization. Additional morphological studies of the inclusion of poloxamer 188 in LNPs suggests that the excipient lowers aerosolization induced fusion or aggregation of particles without altering the internal structure. Our results indicate that poloxamer 188 can support aerosolized mRNA LNP delivery by maintaining LNP size and significantly enhancing therapeutic nucleic acid delivery to lung cells.

Received 28th February 2025,
Accepted 18th June 2025

DOI: 10.1039/d5pm00061k

rsc.li/RSCPharma

1. Introduction

Delivery of nucleic acids is promising for treatment of infections, vaccination, and gene editing of disease-causing mutations. Nucleic acids, such as messenger RNA (mRNA), are highly tunable and upon delivery into cells, encode instructions for cells to produce their own proteins of interest for therapy, enabling the cell to act as a "living pharmacy".[1] However, when free mRNA is delivered *in vivo*, it is subject to degradation by nucleases and can trigger the host immune system, greatly diminishing therapeutic dosing.[2–5] Therefore, it is imperative that the mRNA is encapsulated within a carrier such as a lipid nanoparticle (LNP), polymeric nanoparticle, or viral vector.[1] Of particular interest, LNPs have risen to popularity as carriers for mRNA due to the development of mRNA LNP vaccines against SARS-CoV-2 during the COVID-19 pandemic.[6–8] Many other mRNA LNP formulations have been created for treatment of cancer, infectious diseases, and genetic diseases.[9–20]

Patients with genetic lung diseases such as cystic fibrosis, alpha-1 antitrypsin deficiency, and primary ciliary dyskinesia are strong candidates for mRNA LNP therapies to correct disease-causing mutations using gene replacement or gene editing technologies.[21,22] Treatments for genetic lung diseases can be directed to the lungs *via* systemic or local delivery. Systemic delivery often consists of intravenous injection which allows for immediate bioavailability of the therapeutic at the site of action but faces many challenges such as hepatic uptake, binding of plasma proteins to the surface of the LNP which limits cellular uptake, and off-target uptake in other organs.[23–30] Local delivery of therapies involves directing treatment to the lungs *via* inhalation. Inhaled delivery remains a promising avenue to deliver LNPs to the lungs as the therapy

[a]*Department of Biomedical Engineering, The University of Texas at Austin, Austin, Texas, USA*
[b]*Walker Department of Mechanical Engineering, The University of Texas at Austin, Austin, Texas, USA*
[c]*Division of Molecular Pharmaceutics and Drug Delivery, College of Pharmacy, The University of Texas at Austin, Austin, Texas, USA. E-mail: dghosh@austin.utexas.edu*
† Electronic supplementary information (ESI) available. See DOI: https://doi.org/10.1039/d5pm00061k

can bypass liver and kidney clearance and increase the concentration of the therapeutic in the area of interest.[30] In addition, biodistribution studies have shown that lipid-based carriers remain in the lungs with no noticeable uptake into circulation, reducing off target effects in all other organs.[19,31] Inhaled LNP therapies are transformed from a liquid storage form into aerosol droplets *via* multiple aerosolization methods including nebulization. However, aerosolization can induce shear stress on the structure of the LNP, significantly reducing mRNA delivery and causing fusion or aggregation of particles.[32–37] As a result, it is critical to better maintain the LNP structure during aerosolization to retain mRNA for effective delivery.

The structure of most LNPs generally consists of four main components: (1) ionizable lipids, which are neutrally charged at physiological pH but become protonated in acidic environments to facilitate endosomal escape; (2) phospholipids, also referred to as helper lipids, that aids in maintaining the LNP structure and enhancing endosomal escape; (3) polyethylene glycol (PEG)-lipids that contributes to particle size, steric hindrance, and colloidal stability; and (4) cholesterol, which helps maintain membrane integrity and rigidity.[38] Multiple aerosolized mRNA-LNP clinical trials for genetic diseases in the lungs have been initiated within the last five years but have been met with limited success or have yet to be evaluated for effectiveness, indicating a need for further development of aerosolized mRNA LNPs.[39–43] Current research has moved to improve the efficacy of aerosolized LNPs by screening novel lipid structures, altering buffer solutions, or optimizing lipid components.[20,32,33,36,44–46] A few research groups have added an additional component to the base LNP formulation such as a permanently cationic lipid or an inactive substance used to aid delivery, traditionally termed an excipient.[35,47,48] The excipients used in previous studies improved mRNA expression after aerosolized delivery compared to LNPs without excipients, but it is unclear if this improvement in delivery was due to the excipient or to the change in buffer system.[47,48] There was an observable size change in the LNPs after aerosolization in both studies, which indicates the LNPs are still susceptible to shear stress even in the presence of excipients. An important observation in these studies is that the excipient-doped LNPs were only tested for transfection after aerosolization. It is important to measure changes in mRNA LNPs both before and after aerosolization to determine if there are undocumented morphological changes, which would reduce the delivered dose and ultimately, adversely affect therapeutic efficacy.

We will explore changes in LNP structure during aerosolization using a design of experiments (DOE) approach. This approach allows us to systematically identify select excipients that can help retain the physicochemical properties of mRNA LNPs before and after nebulization and consequently, improve mRNA delivery. DOE is used to condense a large multiparameter space and systematically evaluate relationships between input variables and responses.[32,44,48] Here, we use DOE to draw conclusions between factors and identify the optimal conditions for excipient-doped LNPs. Excipients have been previously shown to provide chemical and physical stability to inhaled products, making them a promising route for stabilizing aerosolized LNPs.[49] As part of our study, excipients were added to our previously optimized aerosolized mRNA LNP composition to further improve its ability to deliver mRNA after nebulization.[33] By characterizing the effect each excipient had on the mRNA LNP size, morphology, permeation, and mRNA transfection after aerosolization, we were able to identify a lead excipient candidate able to best retain the performance of mRNA LNPs for aerosolized delivery.

2. Materials and methods

2.1 Materials

The ionizable lipid SM-102 (heptadecan-9-yl 8-{(2-hydroxyethyl) [6-oxo-6 (undecyloxy)hexyl]amino}octanoate, BP-25499) was purchased from BroadPharm. The helper lipid DPPC (1,2-dipalmitoyl-*sn-glycero*-3-phosphocholine, 850355) was purchased from Avanti Polar Lipids. The polyethylene glycol (PEG) anchored lipid, DMPE-PEG 2000 (1,2-dimyristoyl-*sn-glycero*-3-phosphoethanolamine-*N*-[methoxy(polyethylene glycol)-2000], PM-020CN), was purchased from NOF America Corporation. Cholesterol was purchased from Sigma-Aldrich (C3045).

Excipients L-Arginine HCl ((*S*)-2-amino-5-guanidinopentanoic acid hydrochloride, A121639) and Leucine (H-Leu-OH, A197119) were purchased from AmBeed. Poloxamer 188 (poly(ethylene glycol)-*block*-poly(propylene glycol)-*block*-poly(ethylene glycol), 15759) was purchased from Sigma-Aldrich. Poloxamer 407 (Pluronic®-F127, 59000) was purchased from Biotium. Methylparaben, NF (ME163) and propylparaben, NF, BP, EP (PR133) were purchased from Spectrum Chemicals. Polysorbate 20 (Tween 20™ Ultrapure, J20605) was purchased from Thermo Scientific Chemicals. Branched PEG (4-arm PEG Acrylate 20K, 4ARM-ACLT) was purchased from JenKem Technology.

2.2 Nanoluciferase mRNA

Nanoluciferase (NLuc) mRNA was prepared as previously described.[19,33] A custom NLuc gene block from Twist Biosciences encoding sequences for a T7 promoter, 5′ UTR, codon-optimized NLuc, and 3′ UTR was amplified using polymerase chain reaction (PCR). Detailed sequence information is given in the ESI.† NLuc mRNA was transcribed using the AmpliScribe™ T7-Flash™ Transcription Kit (Lucigen, ASF-3507). The mRNA was purified after transcription using RNA Clean and Concentrator-100 (Zymo, R1019). Following purification, a cap1 structure was added to the 5′ end using the Vaccinia Capping System (New England Biolabs, M2080S) and mRNA Cap 2′-*O*-methyltransferase (New England Biolabs, M0366S). A 3′-poly(A) tail approximately 100 bp long was added using *E. coli* poly (A) polymerase (New England Biolabs, M0276L). Capped and polyadenylated NLuc mRNA was purified again using RNA Clean & Concentrator-100. The NanoDrop One (Thermo Fisher Scientific Inc.) was then used to determine mRNA concentrations, and aliquots were stored at −80 °C until use.

2.3 Formulation of lipid nanoparticles (LNPs)

LNPs were formulated using microfluidic mixing of the organic and aqueous phases, as described previously.[32,33] The organic phase contained 10 mg mL^{-1} SM-102, DPPC, DMPE-PEG and cholesterol in 100% ethanol at molar ratios of 0.45, 0.20, 0.01, and 0.34, respectively. The aqueous phase consisted of mRNA diluted in 50 mM sodium citrate buffer at a pH of 3.0. The organic and aqueous phases were combined using the NanoAssemblr Benchtop Microfluidic System (Cytiva) at a respective ratio of 1 : 3 and a flow rate of 9 mL per minute. The ratio of amine groups (N) present in lipids to the phosphate groups (P) present in mRNA cargo was previously optimized.[33] LNPs were formulated at an N : P ratio of 5.67 and at varying mRNA concentrations ranging from 37.5 ng μL^{-1} to 50 ng μL^{-1}. After formulation, LNPs were dialyzed against 1× PBS, pH = 7.4 overnight using 3 mL Slide-A-Lyzer™ G2 Dialysis Cassette with a 10 k Da molecular weight cutoff (Thermo Fisher Scientific, 87730). Formulations were stored at 4 °C until use.

2.4 Addition of excipients post-formulation

Arginine, leucine, poloxamer 188, poloxamer 407, methylparaben, propylparaben, and polysorbate 20 were dissolved in 1× PBS at a concentration of 20 mg mL^{-1} in separate microcentrifuge tubes (Fisherbrand™ Premium Microcentrifuge Tubes, 05-408-129). Branched PEG was dissolved at a concentration of 100 mg mL^{-1} in 1× PBS. All excipients were then vortexed until visibly dissolved. The leucine, poloxamer 407, methylparaben, and propylparaben were heated at 65 °C for 17 hours until dissolved.

A single LNP formulation was divided into separate microcentrifuge tubes in preparation for excipient addition. The 20 mg mL^{-1} stocks of arginine, leucine, poloxamer 188, poloxamer 407, methylparaben, propylparaben, and polysorbate 20 were added to LNPs after dialysis at varying concentrations ranging from 0–20% (%w/v) according to the DOE. The 100 mg mL^{-1} stock of branched PEG was added to LNPs at a 2% concentration. All samples were brought to equal volumes using 1× PBS to ensure samples contained equal mRNA concentrations.

2.5 Aerosolization

LNPs with and without added excipients were nebulized individually using an Aerogen Solo vibrating mesh nebulizer (Aerogen Ltd). The nebulizer was washed with 2 mL of 1× PBS between each sample. The temperature of the nebulizer was monitored throughout nebulization of each sample using a FLIR T620 infrared camera (Teledyne FLIR). Temperature readings were focused on the piezoelectric element and mesh of the nebulizer body to directly monitor temperature of the samples passing through the mesh during nebulization. Nebulized formulations were collected in chilled microcentrifuge tubes for testing.

2.6 Characterization of LNPs

2.6.1 Size and polydispersity index. Size and polydispersity index (PDI) of LNPs with and without excipient addition were measured separately by dynamic light scattering using the Zetasizer Nano-ZS (Malvern Instruments). All samples were diluted using 1× PBS to a final mRNA concentration of 1.25 ng μL^{-1} in 100 μL and measured in a UV-Cuvette Micro (BrandTech Scientific, 759200). Samples were measured in triplicate and results are expressed as the mean ± standard deviation.

2.6.2 Zeta potential. Zeta potential of LNPs with and without excipient addition was measured using the Zetasizer Nano-ZS (Malvern Instruments). All samples were diluted using 0.1× PBS to a final mRNA concentration of 1.5 ng μL^{-1} in 780 μL and measured using a Folded Capillary Zeta Cell (Malvern Panalytical, DTS1070). Samples were measured in triplicate and results are expressed as the mean ± standard deviation.

2.6.3 Osmolality evaluation. The osmolality (mOsm kg^{-1}) of LNP samples with and without excipients was measured using a μOsmette Automatic Osmometer (Precision Systems Inc., model 5004). The μOsmette was set to the first range (0–2000 mOsm kg^{-1}) and calibrated using a 500 mOsm kg^{-1} osmometry standard (Precision Systems Inc., 2105). The probe was wiped clean between each standard and sample. Samples were transferred into separate Disposable Sample Tubes (Precision Systems Inc., 2023) at a volume of 50 μL for osmolality evaluation. Samples were measured in triplicate and results are expressed as the mean ± standard deviation.

2.6.4 Encapsulation efficiency. The Quant-it RiboGreen RNA Kit (Thermo Fisher Scientific, R11490) was used to evaluate encapsulation of mRNA in all LNP samples. A 1× Tris-EDTA (TE) buffer was prepared by diluting 20× TE buffer (Thermo Fisher Scientific, R11490) with UltraPure™ DNase/RNase-Free Distilled Water (Invitrogen, 10977015). A 2% Triton buffer was prepared by diluting Triton X-100 (Thermo Fisher Scientific, BP151-100) in 1× TE buffer. The high range standard curves were prepared at concentrations of 1–500 ng mL^{-1} in both 1× TE and 2% Triton with ribosomal RNA contained in the kit. All LNP samples were diluted 50-fold in both 1× TE and 2% Triton buffers. Samples and standards were plated at a volume of 100 μL in triplicate on a 96-well Black/Clear Flat Bottom Polystyrene Microplate (Corning, 3631) and incubated at 37 °C for 10 minutes. A 200-fold dilution of RiboGreen RNA Reagent was added to each sample and standard at a volume of 100 μL. Fluorescence was then measured using BioTek Synergy H1 multiplate reader (Agilent Technologies) at 485 nm excitation and 528 nm emission. Encapsulation efficiency (EE%) was calculated using eqn (1):

$$EE\% = \left(1 - \frac{F_{\text{free RNA}}}{F_{\text{total RNA}}}\right) \times 100 \quad (1)$$

Here, $F_{\text{free RNA}}$ and $F_{\text{total RNA}}$ correspond to the fluorescent signal of the free RNA in 1× TE buffer and the fluorescent signal of the total RNA found in the 2% Triton buffer, respectively.

2.7 Air–liquid interface cell culture

Calu-3 cells (American Type Culture Collection, HTB-55) between passages 10–20 were centrifuged at 350*g* for

5 minutes and resuspended in 89% 1× Minimum Essential Medium (MEM) containing Earle's salts and L-glutamine (Corning, 10-010-CV) with added 10% Fetal Bovine Serum (Gemini Bio, 100–106) and 1% Penicillin/Streptomycin. The cells were seeded at a density of 300 000 cells per well on the apical side of ThinCert Cell Culture Inserts for 24-well plates, made of PET with 0.4 μm pores (Greiner Bio-one International, 662641). Media was added on the basolateral side of the transwell at a volume of 500 μL, and on the apical side to reach a volume of 200 μL. The cells were incubated at 37 °C in 5% CO_2 atmosphere. Media was replaced on both the basolateral and apical side of the transwell every 2–3 days. After 6 days the media on the apical side was removed when the cells reached >85% confluency and cells were cultured at air–liquid interface (ALI) as previously described.[33] Media was replaced on only the basolateral side every 2–3 days until testing 7–9 days after starting ALI culture.

Transepithelial electrical resistance (TEER) values were measured using a Millicell ERS-2 Voltohmmeter (Millipore Sigma, MERS00002). Cell media was maintained on the basolateral side of the transwell at a volume of 500 μL, and 200 μL of fresh cell media was added to the apical side of the transwell. Cells were equilibrated at room temperature for 15 minutes. TEER measurements were recorded for four representative wells throughout the air-lifting process. Values were calculated by subtracting the resistance of the blank transwell without cells and multiplied by the surface area. Cells were air-lifted when TEER values reached >400 Ω cm^2 in cell media.

2.8 *In vitro* transfection

LNP samples were added to the apical side of Calu-3 cells cultured at ALI at an NLuc mRNA dose of 500 ng per well. Opti-MEM Reduced Serum Media (Gibco, 31-985-062) was added to the apical side until the total volume of sample and media was equal to 50 μL to cover the entire apical surface area. Calu-3 cells were incubated with LNPs at 37 °C in 5% CO_2 for 24 hours. Media was removed from the basolateral side of the transwell. The LNP samples were then collected from the apical side of each transwell and placed in separate microcentrifuge tubes. Cells were washed with 100 μL 1× PBS and the wash solution was transferred into the corresponding sample microcentrifuge tubes. Cells were scraped from the apical surface of the transwell using a micropipette and collected in their corresponding microcentrifuge tubes. The cells were centrifuged at 300*g* for 3 minutes and resuspended in 100 μL of fresh media. Resuspended cells were transferred to a 96-well white flat bottom polystyrene microplate (Corning, 3912). Nano-Glo substrate from the Nano-Glo® Luciferase Assay System (Promega Corporation, N1110) was diluted 50-fold using the Nano-Glo buffer and 100 μL was added to each sample using a multichannel pipette. Samples were incubated for 3 minutes at room temperature before analysis with BioTek Synergy H1 multiplate reader (Agilent Technologies) using the luminescent fiber setting. Samples were measured in triplicate and results are expressed as the mean ± standard deviation.

2.9 Lucifer yellow barrier assay

LNP samples were added at a dose of 600 ng NLuc mRNA per well to the apical side of Calu-3 cells cultured at ALI. In addition, excipients in 1× PBS (without LNPs) were added to separate wells to monitor the impact of excipients on cell monolayers. The Calu-3 cells were incubated with samples at 37 °C in 5% CO_2 overnight (~17 hours). Cell media was removed from the basolateral side of the transwell. The basolateral side was washed with 900 μL of prewarmed Hanks' Balanced Salt Solution (HBSS), which was removed, and fresh HBSS was then added at a volume of 900 μL. Lucifer Yellow CH dilithium salt (MedChemExpress, HY-128692) was dissolved in HBSS at a concentration of 100 μg mL^{-1} and 200 μL was added to the apical side of each transwell. The cells were incubated at 37 °C in 5% CO_2 with the lucifer yellow fluorescent dye for 2 hours. During incubation, a 100% standard was prepared by mixing 200 μL of the lucifer yellow solution with 900 μL of HBSS. Serial dilutions were then performed by mixing 500 μL of the previous standard with 500 μL of HBSS to obtain standards of 50, 25, 12.5, 6.25, 3.12, 0.78, and 0.39%. After the 2 hour incubation, the solution on the basolateral side of each transwell was mixed using a pipette and 100 μL was retrieved from each well. The samples from the basolateral side of the membrane and standards were plated at a volume of 100 μL in duplicate on 96-well Black/Clear Flat Bottom Polystyrene Microplates (Corning, 3631). Fluorescent intensity of the 96-well plates was read using the BioTek Synergy H1 multiplate reader (Agilent Technologies) at 485 nm excitation and 535 nm emission. The duplicates were averages and the standard curve was used to calculate the estimated percent pass-through of lucifer yellow from the apical side to the basolateral side of the membrane using the relative fluorescence values. Immediately after, the TEER values were taken for all transwells. TEER values were measured in 900 μL prewarmed HBSS on the basolateral side and 200 μL HBSS on the apical side of the transwells. TEER values were measured in triplicate wells and results are expressed as the mean ± standard deviation.

2.10 Cryo-electron microscopy imaging

Images from cryo-electron microscopy (Cryo-EM) were acquired by the Sauer Structural Biology Laboratory at The University of Texas at Austin. LNPs were concentrated to a lipid concentration of 22 mg mL^{-1} using Amicon® Ultra Centrifugal Filters, 10 kDa MWCO (MilliporeSigma, UFC801008/UFC501008) prior to the addition of excipients. Excipients were added to LNPs and nebulized immediately before imaging. Vitrification of each sample was performed using a Vitrobot Mark IV. LNP samples were placed on copper 200 mesh grids with lacey carbon film and a continuous layer of ultrathin carbon at a volume of 2.2 μL with a blot time ranging from 5–11 seconds. After vitrification, sample grids were maintained at a temperature below −170 °C. Imaging was performed on a Glacios Cryo-Transmission Electron Microscope (Thermo Fisher Scientific) operating at 200 kV equipped with a Falcon 4 Direct Electron Detector (Thermo

Fisher Scientific). Images were acquired at a dose rate of 1.48 e^{-} $Å^{-2}$ s^{-1}, an exposure time of 20.2 seconds, a total exposure of 30 e^{-} $Å^{-2}$, and a pixel size of 1.913 Å per pixel. Resulting images were processed using ImageJ to remove noise, enhance contrast, and correct illumination.[50]

2.11 Small-angle X-ray scattering

Small-angle X-ray scattering (SAXS) measurements were performed at the Cornell High Energy Synchrotron Source (CHESS) at beamline 7A using an Eiger 4 M detector. The sample-to-detector distance was 1731 mm, and the X-ray energy was 12.39 keV. The experiments were conducted in a quartz capillary with a diameter of 1.55 mm and a wall thickness of 10 μm. The scattering vector range (q) was 0.008–0.33 $Å^{-1}$. LNPs were concentrated to a lipid concentration of 6.3 mg mL^{-1} using Amicon® Ultra Centrifugal Filters, 10 kDa MWCO (MilliporeSigma, UFC801008/UFC501008) prior to the addition of excipients. Excipients were added accordingly, and 1% glycerol was added to both samples. A total sample volume of 40 μL was used for each measurement, and an automated liquid sample loader was employed to ensure consistent sample handling and minimize radiation damage. Igor Pro (WaveMetrics) was used to plot the SAXS profile.

Peak deconvolution was performed using OriginPro 2025 (OriginLab). Since the observed peak was asymmetrical, a two-peak deconvolution approach with a Gaussian fit was applied, described by eqn (2):

$$y = y_0 + Ae^{-\frac{(x-x_c)^2}{2w^2}} \quad (2)$$

Here y_0 represents the baseline offset, A is the peak amplitude, x_c is the center of the peak (peak position), and w is the width parameter, related to the full width at half maximum (FWHM). The ordering distance was calculated as $\frac{2\pi}{q}$ following Bragg's Law.

2.12 Statistical analysis

A DOE approach was employed to design the excipient screening using JMP 17 (JMP Statistical Discovery LLC). The DOE was created using a two-factor definitive screening design with excipient type and excipient concentration as the factors. All data analyses for statistical significance was done in GraphPad Prism (version 10.4.1). Data values were presented as mean ± standard deviation (SD). All p-values were calculated using an ordinary one-way or two-way ANOVA assuming normal distribution and an alpha value of 0.05, where $*p < 0.05$, $**p < 0.01$, $***p < 0.001$, and $****p < 0.0001$ were considered statistically significant.

3. Results and discussion

3.1 DOE excipient screening

We selected our excipients based on one of two criteria; the excipients (1) are currently used in marketed inhaled products approved by the Food and Drug Administration (FDA) to enhance the physical or chemical stability of the active pharmaceutical ingredient and/or (2) have shown promise to stabilize lipid membranes. The first criteria includes parabens and polysorbates.[51] Parabens such as methylparaben and propylparaben have been included in approved inhaled medications and have shown increased surface shear resistance in lipid monolayers.[51,52] Polysorbate 20 is a sorbitan functionalized with poly(ethylene) glycol (PEG) that is approved for inhalation use, and previous research has shown that 3% polysorbate 20 enhances LNP transfection in targeted gene delivery.[51,53] The combination of safety and observed enhancement of lipid-based structure characteristics from previous research indicates that parabens and polysorbate 20 are strong candidates to stabilize aerosolized LNP formulations.

The second criteria supports the use of excipients that are not in currently approved inhalation products but have shown promising stabilizing properties for inhaled biological medications, namely amino acids and poloxamers.[51] Amino acids such as arginine and leucine have been shown to improve surface activity, charge density, and stabilize proteins against thermal stress.[51,54] Previous groups found that amino acid modified lipids aided in delivery of siRNA and that L-amino acids incorporate directly into the membrane of liposomes.[55,56] Poloxamers, such as poloxamer 188 and poloxamer 407, are block copolymers that are comprised of a central poly(oxypropylene) (PPO) molecule that is flanked on both sides by two chains of poly(oxyethylene) (PEO).[57] Poloxamers have similar structures but vary in the number of PPO and PEO units and their molecular weights. Poloxamer 188 contains around 80% PEO units and 20% PPO units, whereas poloxamer 407 contains around 70% PEO and 30% PPO units.[57] Poloxamers have been used to repair broken cell membranes by increasing lipid packing density and improve gene transfection, making poloxamers an ideal excipient for LNP stabilization.[58,59] Methylparaben, propylparaben, polysorbate 20, arginine, leucine, poloxamer 188, and poloxamer 407 were chosen for our excipient screening as they adhered to one or both of our defined criteria to improve LNP stability during aerosolization.

The excipients were screened on a single four-component LNP formulation that we had previously optimized as an initial formulation to improve aerosolized LNP delivery.[33] This LNP composition, labeled as B1, was used as the base formulation and a control throughout our excipient screening. All excipients for the screening were added to aliquots of B1 after formulation and buffer exchange (Fig. 1). For experimental design, we used a DOE approach to systematically investigate the effect of excipients on the properties of aerosolized B1 mRNA-LNPs and draw conclusions between factors. A two-factor definitive screening DOE was employed with excipient type and excipient concentration as the designated factors (Table S1†). We performed a thorough investigation of the literature to rationally narrow the excipient type screening. Excipient concentration was chosen to be between 0–20% w/v as 20% was the highest concentration of excipients in inhaled

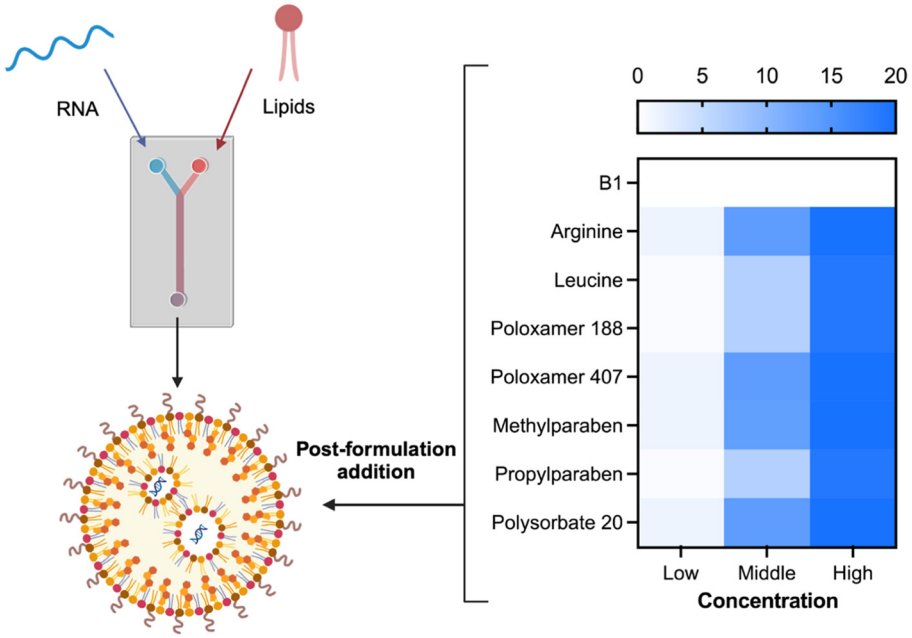

Fig. 1 Post-formulation addition of excipients to lipid nanoparticles. RNA and lipids are combined *via* microfluidic mixing to formulate a lipid nanoparticle. Excipients are added to the lipid nanoparticles at a low, middle, and high concentration as depicted by the heat map.

formulations that could be found in the literaure.[51] Using JMP statistical software, we created a screening design output with 21 groups consisting of a low, medium, and high concentration for each excipient (Table S2†).

3.2 Characterization of excipient-doped LNPs

Throughout consecutive nebulization of all 23 samples, we monitored the nebulizer mesh with an infrared camera for any possible temperature changes that could change particle characteristics (Fig. S1†). Temperature readings were taken at the mesh of the nebulizer at the start of nebulization for each sample. The temperature of the nebulizer at the start of aerosolization for each sample was on average 25.74 ± 0.29 °C for all 23 samples. The calculated change in temperature of the nebulizer mesh, relative to the first sample (labeled B1), was on average 0.67 ± 0.26 °C for the remaining 22 samples. This temperature variation is less than the previously reported 2 °C average for the MicroBase Pocket AirNeb Mini Portable Nebuliser, a different vibrating mesh nebulizer on the market.[60] There was a minimal increase in temperature of the vibrating mesh nebulizer when used repeatedly. This suggests that there will be minimal differences in LNP physical properties due to temperature changes in samples nebulized later compared to samples nebulized first.

Two of our criteria for successful aerosolized excipient-doped LNPs are minimal particle size and polydispersity changes before and after nebulization. Dynamic light scattering (DLS) was employed to measure LNP size and polydispersity index (PDI) before and after aerosolization (Fig. 2 and 3, respectively). DLS is considered a good estimator of a particle's ability to remain suspended in solution with minimal aggregation.[61] Previous research has reported more than a 1.5-fold size increase following aerosolization of mRNA LNPs without excipients, which supports the size changes seen in our B1 LNP without excipients.[32,33,47,48] Our results indicate that upon the addition of 19% P188, 14% P407, 20% P407, 14% PS20, or 20% PS20 to LNPs, there was no significant change in LNP size before and after aerosolization. However, we observed that the PS20 samples had low signal count rates during DLS measurements, likely due to PS20 destroying LNP structures. The lack of size change in P188 and P407 samples indicate that the presence of poloxamer may help maintain colloidal stability of LNPs during high shear situations such as aerosolization.[62,63] In addition, our use of P188 in 1× PBS buffer showed better size retention after aerosolization than the previously shown use of P188 in HEPES buffer.[47]

Clinically used LNPs are typically between 50–100 nm in size.[64,65] Our LNPs with and without excipients displayed an average size of less than 100 nm before aerosolization. After aerosolization, we found that B1 without excipients and B1 samples with arginine, leucine, methylparaben, and propylparaben had LNP sizes over 140 nm. Studies have indicated that LNP sizes larger than 120 nm result in lower nucleic acid expression compared to LNPs smaller than 120 nm.[65] We sought to correlate the size changes seen in our LNP samples before and after aerosolization with efficacy of nucleic acid delivery in section 3.3. Interestingly, the 19% P188 LNP resulted in an average diameter of 82.1 nm after aerosolization, which is the smallest aerosolized particle size excluding P407 and PS20. The size retention seen in P188-doped LNPs could be attributed to the previously described ability of poloxamers to reseal damaged membranes.[58,66] P188 could be resealing

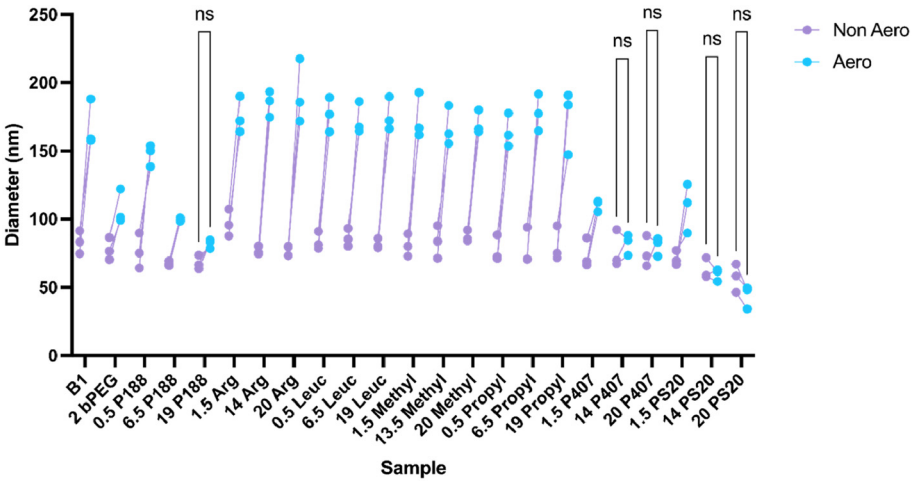

Fig. 2 Dynamic light scattering measurements of LNP diameters before and after aerosolization. B1 is the non-excipient control for the excipient screening. Significance is determined between non-aero and aero samples (n = 3; ns = no significance; two-way ANOVA with alpha = 0.05).

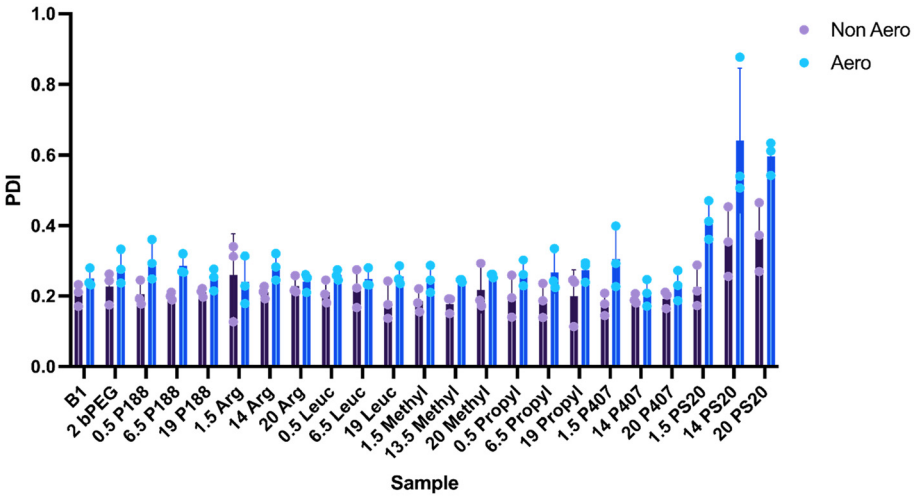

Fig. 3 Polydispersity of excipient-doped LNPs before and after aerosolization (n = 3; mean ± standard deviation [SD]). B1 is the non-excipient control for the excipient screening. PDI is polydispersity index.

the damage induced in the lipid membrane of LNPs by aerosolization to maintain the particle size throughout aerosolization.

Zeta potential was measured to understand the charge of LNPs with the addition of excipients (Fig. 4). Previously developed LNPs for aerosolized delivery have shown varying zeta potentials within the range of 20 to −10 mV before aerosolization.[32,33,48] The non-excipient and excipient doped LNPs tested displayed zeta potential values between 0.5 and −10 mV before aerosolization and −2.5 and −20 mV after aerosolization. The 19% P188, 1.5% Arg, 14% Arg, 0.5% Leuc, 6.5% Leuc, 20% methyl, 0.5% propyl, 6.5% propyl, and 19% propyl samples displayed a statistically significant change (p < 0.05) in zeta potential values before and after nebulization. In particular, 19% P188 possessed a zeta potential of −6.4 mV before nebulization, which decreased to −12.5 mV after nebulization. Nanodispersions that contain nonionic surfactants, such as P188, are typically more colloidally stable as zeta potential values approach ±20 mV.[67] Therefore, after nebulization, the decrease in zeta potential seen in 19% P188, 1.5% Arg, 14% Arg, 0.5% Leuc, 6.5% Leuc, 20% methyl, 0.5% propyl, 6.5% propyl, and 19% propyl suggest there is a shift toward colloidal stability.

We measured the osmolality of our LNP samples with and without excipients (Fig. 5). The osmolality of our control LNP without excipients, B1, was 276 mOsm kg^{-1}, which is within the range of an isotonic solution (275–295 mOsm kg^{-1}).[68] Here, LNP samples, upon the addition of the following excipients, were isotonic: 2% bPEG, 0.5% P188, 6.5% P188, 19% P188, 1.5% Arg, 0.5% Leuc, 1.5% methyl, 0.5% propyl, 1.5% P407, 14% P407, 20% P407, 1.5% PS20, 14% PS20, and 20% PS20. The addition of other excipients such as 14% Arg, 20%

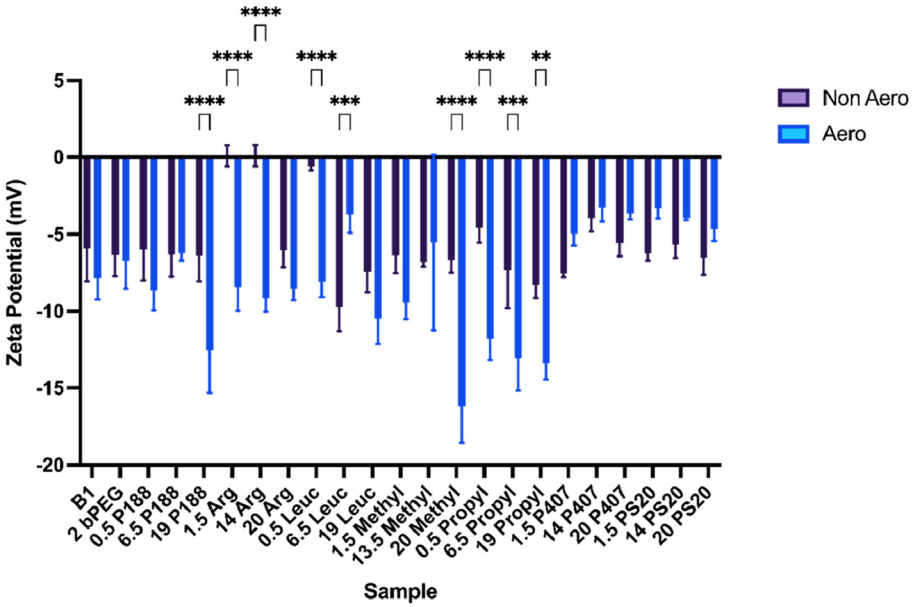

Fig. 4 Zeta potential measurements of non-excipient (B1) and excipient-doped LNPs before and after aerosolization (n = 3; mean ± standard deviation [SD], $^{**}p < 0.01$, $^{***}p < 0.001$, $^{****}p < 0.0001$; two-way ANOVA with alpha = 0.05).

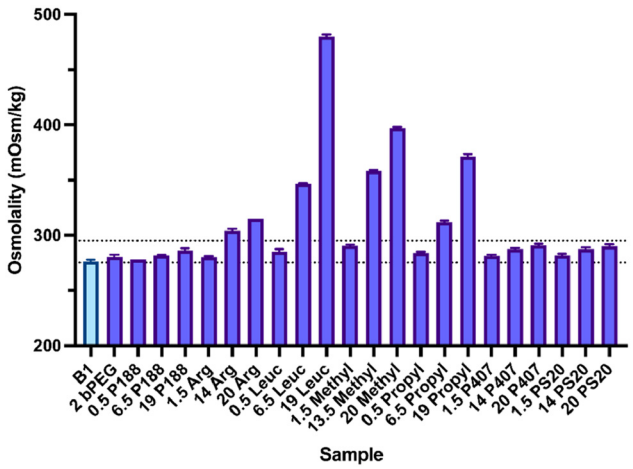

Fig. 5 Osmolality measurements of non-excipient B1 (light blue) and excipient-doped LNPs (dark blue). The indicated range from 275–295 mOsm kg^{-1} marks the lower and upper bounds of isotonic solutions (n = 3; mean ± standard deviation [SD]).

Arg, 6.5% Leuc, 19% Leuc, 13.5% methyl, 20% methyl, 6.5% propyl, and 19% propyl resulted in hypertonic solutions (Fig. 5). The LNP samples containing arginine, leucine, methylparaben, or propylparaben displayed concentration dependent increases in osmolality, where the solutions became more hypertonic as the concentration of excipient increased. Solutions that are clinically administered to the lungs typically consist of isotonic solutions.[69] Hypotonic solutions are often not used as they can cause reduced lung function.[68,70] In contrast, hypertonic solutions have been used in the treatment of certain lung diseases such as cystic fibrosis to clear thick mucus buildup.[71] Based on the osmolality of our LNPs with the addition of excipients, our samples are safe for patient use, with most preparations being isotonic. The remaining hypertonic preparations can be used for patients presenting with mucus build-up.

Encapsulation efficiency (EE) was measured for our LNP without excipients (B1) and all excipient-doped LNP samples before and after aerosolization (Fig. 6). There was a significant decrease in EE observed in all non-excipient and excipient-doped samples after aerosolization as compared to before nebulization. Before aerosolization, our LNP samples displayed an EE between 75–90%, with the exception of PS20. Specifically, our control LNP without excipients, B1, had an EE of 81.05% before aerosolization and 31.14% after aerosolization, which is comparable to the EE of aerosolized LNPs in 1× PBS shown in previous studies.[32,33] The 2.6-fold decrease of mRNA encapsulation after nebulization of B1, as compared to before nebulization, was caused by an aerosolization induced loss of mRNA. The 6.5% and 19% P188 doped LNP samples had the highest EE after aerosolization, at an average of about 50% mRNA encapsulated after nebulization. The EE of aerosolized 6.5% and 19% P188 doped LNPs is 1.6-fold higher than our aerosolized LNP without excipients, B1. However, there is still an observable difference in EE before and after aerosolization due to aerosolization induced loss of mRNA in the 6.5% and 19% P188 doped LNPs. We also observed that all three excipient-doped LNP samples containing PS20 resulted in 0% encapsulation before nebulization. We hypothesize that the presence of PS20 in LNP buffers may adversely impact the LNP structure and lead to a subsequent release of mRNA.

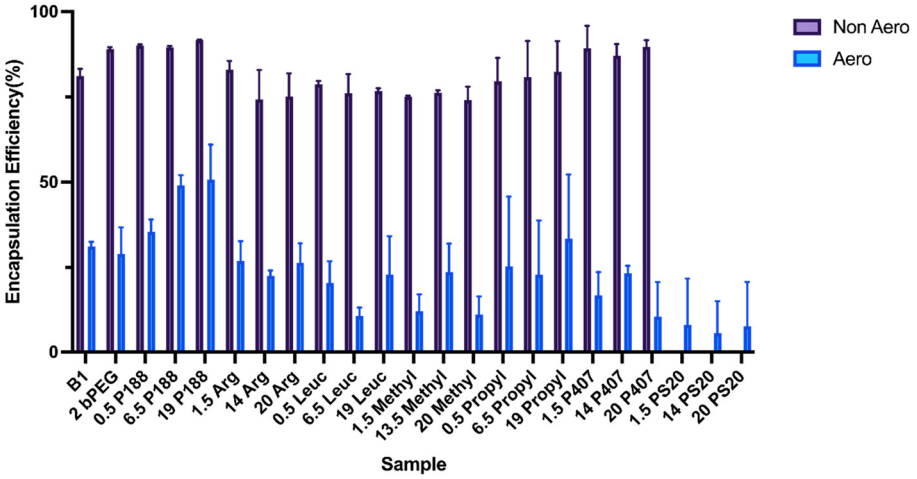

Fig. 6 Encapsulation efficiency of LNPs with and without excipients before and after aerosolization (n = 3; mean ± standard deviation [SD]). B1 is the non-excipient control for the excipient screening.

3.3 Effect of excipients on cellular uptake of LNPs

We encapsulated NLuc mRNA, a luminescent reporter molecule that is ~150× more sensitive than firefly luciferase, within our B1 formulation.[72] We studied LNP mRNA delivery by measuring the luminescence bioactivity of luciferase expression from delivered NLuc mRNA. The B1 formulation was split into 23 different tubes and arginine (Arg), leucine (Leuc), poloxamer 188 (P188), poloxamer 407 (P407), methylparaben (methyl), propylparaben (propyl), polysorbate 20 (PS20), branched PEG (bPEG), and/or 1× PBS was added at varying concentrations. We nebulized half of each sample and then added both non-aerosolized and aerosolized LNP samples to Calu-3 cells cultured at ALI, which is a better representative model of the lung epithelial barrier compared to submerged cell cultures.[73] We chose this cell type as we wanted to test delivery in lung epithelia that is comparable to the cells present in the human pulmonary tract. We delivered LNPs at a dose of 500 ng to the apical side of the ALI culture. After incubating for 24 hours, we harvested the cells and used a luciferase assay to measure luminescence bioactivity as an indicator of cellular delivery (Fig. 7).

The performance of B1 LNP with or without screened excipients was evaluated before and after nebulization. As seen in

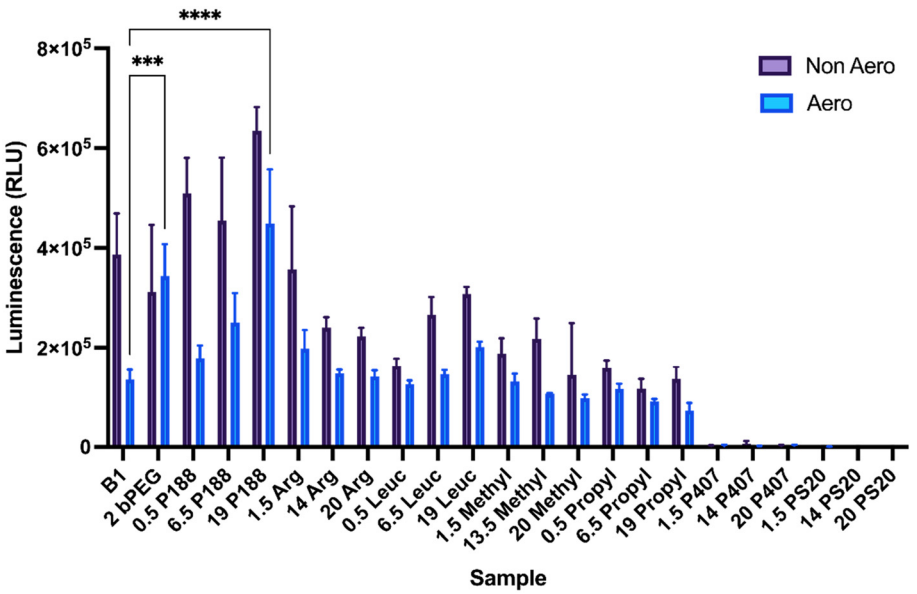

Fig. 7 Excipient-doped LNP cellular expression of bioactivity before and after aerosolization. Graph displays quantification of luminescence 24 hours after NLuc mRNA transfection of Calu-3 cells at air–liquid interface. B1 and 2 bPEG serve as controls for excipient screening. Significance is relative to aerosolized B1 (n = 3; mean ± standard deviation [SD], ***p < 0.001, ****p < 0.0001; two-way ANOVA with alpha = 0.05).

previous literature, our LNP without excipients (B1) had a ~2.3 fold loss of mRNA expression after aerosolization.[32–34] Our best performing excipient-doped LNP, 19% P188, had a 3.3-fold increase in luminescence intensity as compared to aerosolized B1 without excipients. This significant increase in mRNA expression after aerosolization could be due to P188 enhancing passive permeability through lipid monolayers.[74] It has also been suggested that P188 can enhance paracellular permeation.[75] However, we show evidence that P188 does not disrupt tight junctions at our working concentrations in section 3.4. Another excipient-doped LNP, 1.5% Arg, had a higher aerosolized luminescent bioactivity than B1 without excipients. We compared our 19% P188 and 1.5% Arg LNPs to a recently discovered excipient, bPEG, used to stabilize aerosolized LNP formulations.[48] We found that the addition of 2% bPEG to our B1 LNP resulted in a 2.8-fold increase in luminescence after aerosolization compared to B1 without excipients after nebulization. However, our best performing excipient-doped LNP, 19% P188, was 1.2-fold higher in luminescent intensity compared to the 2% bPEG LNP after aerosolization. In addition to the increase in transfection, the size of the 19% P188 LNP was one of the few excipient-doped LNPs that remained under 120 nm after aerosolization (Fig. 2). As stated earlier, particles with less than 120 nm in diameter have been shown to demonstrate improved nucleic acid delivery. Our aerosolized particles that were larger than 140 nm demonstrated a decrease in luciferase activity due to decreased nucleic acid delivery, which has been previous been reported with similarly sized particles.[65] P188 has been described in the literature to improve LNP delivery in HEPES (2-[4-(2-hydroxyethyl)piperazin-1-yl]ethanesulfonic acid) buffer, but the role of the excipient in 1× PBS had yet to be confirmed.[47] We selected 19% P188 and 1.5% Arg doped LNPs as our leading candidates for further testing.

Due to the success of P188, we expanded the range of concentrations tested to determine if there is an increase in luminescence after aerosolization as the concentration of P188 was increased (Fig. S2†). We made a 100 mg mL^{-1} solution of P188 in 1× PBS, which we added to LNPs at concentrations of 3.8% (equivalent to 19% of a 20 mg mL^{-1} P188 solution), 10%, 25%, or 50%. Results indicated a similar 3.0-fold increase in luminescence with the addition of 3.8% 100 mg mL^{-1} P188 compared to B1 without excipients after aerosolization. But there was no significant difference in the relative luminescence between LNPs with either 3.8%, 10%, 25%, and 50% 100 mg mL^{-1} P188. We performed subsequent experiments with 19% 20 mg mL^{-1} P188 (equivalent to 3.8% 100 mg mL^{-1} P188) to minimize the amount of excipient added to the LNP formulation while still achieving maximum mRNA delivery.

Interestingly, we found that the addition of both P407 and PS20 to our B1 LNPs led to minimal luminescence signal (less than 5000 RLU) both before and after aerosolization. The characterization results indicated that P407 likely does not impact the stability of the LNP itself but inhibits cellular uptake. We hypothesize that the lack of cellular uptake is due to the thermoresponsive gelation properties previously displayed by P407 at physiological temperatures.[76] In addition, P407 is less hydrophilic than P188, indicating that hydrophilicity may be a key contributor to the success of excipient-doped aerosolized LNP delivery.[57] Whereas PS20 seems to disrupt the LNP structure according to our characterization results, which may prevent delivery of mRNA into the cells. The remaining excipient-doped LNPs showed no significant difference in luminescent intensity after aerosolization compared to B1 without excipients.

3.4 Effect of excipients on permeability of tight junctions

The immortalized bronchial epithelial cell line, Calu-3, was used to study if non-excipient or excipient-doped LNPs change the permeability of cellular tight junctions. Calu-3 cells are representative bronchial epithelial cells that can grow on porous membranes and form representative tight junctions.[73] We initially took TEER measurements to confirm formation of tight junction after culturing cells at air–liquid interface.[77] Upon conformation that tight junctions were present, we added non-excipient LNPs, excipient-doped LNPs, or excipients without LNPs to separate wells. After an overnight incubation, we added the hydrophilic fluorescent dye lucifer yellow, a solute that can only transport across permeable cell monolayers, to monitor the integrity of the cell monolayer in the presence of excipients. Lucifer yellow was added to the apical side of the transwell for 2 hours, after which we collected a portion of the fluid from the basolateral side of the transwell to measure the amount of lucifer yellow that had passed through the cell monolayer (Fig. 8A). The monolayer barrier is considered intact if there is less than 5% pass-through of the lucifer yellow from the apical side to the basolateral side.[78]

The LNP sample without excipients (B1) served as our benchmark for the impact of LNPs alone on the cell monolayer. The B1 and bPEG wells displayed a lucifer yellow percent pass-through of 0.36% and 0.37%, respectively. In the presence of P188, Arg, Leuc, methyl, propyl, P407, and PS20 excipient-doped LNPs, lucifer yellow had a pass-through ranging from 0.35–1.32%, with the exception of the 20% PS20 (8.25%) LNP sample. Therefore, the P188, Arg, Leuc, methyl, propyl, P407, and PS20 (excluding 20% PS20) excipient-doped LNPs can successfully transfect cells while maintaining the cellular tight junctions. The 8.25% pass-through of the 20% PS20 sample is above the 5% pass-through cutoff for intact monolayers, indicating that the 20% PS20 LNP sample disrupts cellular monolayers. We also tested the permeability of lucifer yellow in the presence of excipients only (Fig. 8B). Without any excipient (PBS buffer only control), lucifer yellow pass-through was 0.30%. Excipients such as bPEG, P188, Arg, Leuc, methyl, propyl, P407, and PS20 in PBS displayed lucifer yellow percent pass-through values between 0.35–0.94%, except for 14% PS20 and 20% PS20. In the presence of 14% PS20 (8.69%) and 20% PS20 (11.77%), lucifer yellow was permeable above the allowable limit for intact cell monolayers. These findings support previous research, which has shown that PS20 can trigger structural remodeling, such as permeabilization and swelling, in lipid membrane based vesicles.[79]

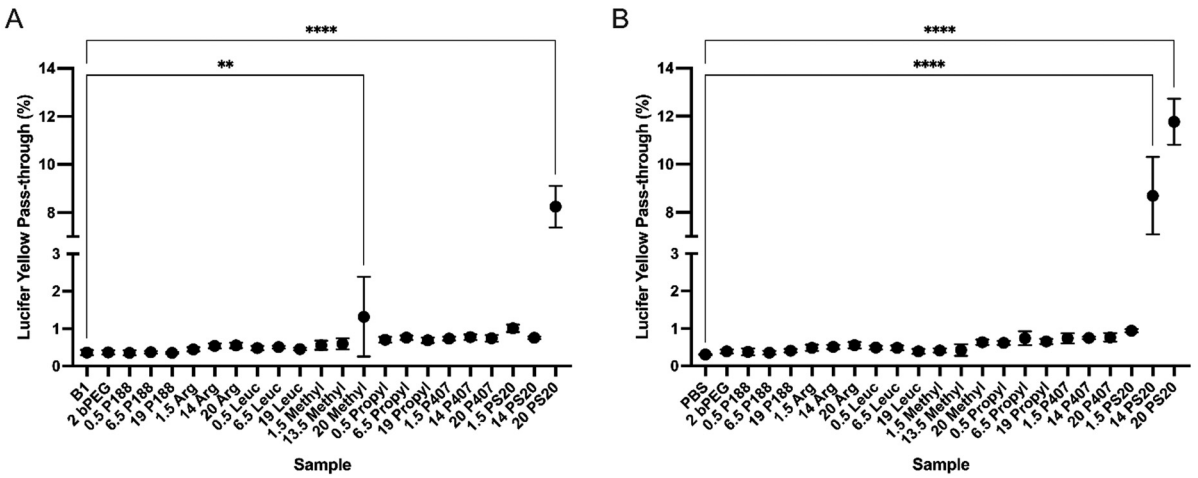

Fig. 8 Percent pass-through of lucifer yellow in Calu-3 cell monolayers dosed with: (A) excipient-doped LNPs, or (B) excipients without LNPs. B1 serves as the control LNP without excipients (A). PBS serves as the control buffer for excipient screening without LNPs (B). (n = 3; mean ± standard deviation [SD], $^{**}p < 0.01$, $^{****}p < 0.0001$; ordinary one-way ANOVA with alpha = 0.05).

TEER measurements were taken after a 24 hour incubation with LNPs and/or excipients (Fig. S2†), and they support our findings with the cell permeability of lucifer yellow. The TEER values of the cell monolayers in transwells 24 hours after dosing of our controls, B1 (excipient + LNP) and PBS (excipient only), were on average 116.70 Ω cm^2 and 120.40 Ω cm^2, respectively. There were no significant changes in TEER values for P188, Arg, Leuc, methyl, and propyl excipient + LNP samples or excipient only samples. There was a significant decrease ($p < 0.05$) in TEER values observed in the 1.5% P407, 14% PS20, and 20% PS20 excipient only sample groups compared to PBS (excipient only). In addition, the 14% PS20 excipient + LNP and excipient only samples demonstrated a significant difference in TEER values. A decrease in TEER is an indicator of a compromised cell barrier and reduction of tight junctions.[77] Our findings with lucifer yellow pass-through and TEER suggest that increasing concentrations of PS20 can lead to increased permeability and disruption of tight junctions. The lack of mRNA delivery (Fig. 7), combined with disruption of cell monolayers, indicates that PS20 is not suitable for excipient-doped LNP delivery. Here, P188, Arg, Leuc, methyl, propyl, and P407 are strong excipient choices to add to LNPs in formulations as they do not cause leakiness and disrupt tight junctions, as evidenced by the lucifer yellow percent pass-through assay and TEER measurements.

The improved transfection rate of P188 and arginine doped LNPs compared to the non-excipient control, B1 (Fig. 7), is not due to paracellular transport, as indicated by lack of paracellular permeability (Fig. 8). Alternatively, other potential mechanisms that may explain the improvement of transfection with 19% P188 and 1.5% Arg include passive permeability through the cell membrane or binding to the cell membrane that results in transient pores in the lipid bilayer.[75,80–82] Previous research on P188 interactions with cell membranes found that P188 can enhance permeability of a poorly permeable drug through a lipid monolayer.[75] Other studies found that arginine can temporarily alter the stability of a cell membrane by binding to the surface of the cell membrane and inducing pores which allow for passive transport through the membrane.[80–82] Importantly, P188 has been deemed safe to use for inhaled delivery, regardless of mechanism, as previous work has shown there was no observed toxicity with P188, even at concentrations comparable to our working concentrations.[83]

3.5 Visualizing LNP morphology changes before and after nebulization

Cryo-EM was used to further visualize the size and polydispersity changes present in our B1 LNP without excipients, as compared to our LNPs with lead excipients 19% P188 and 1.5% Arg (Fig. 9). All other excipient-doped LNPs were excluded as they had not improved the aerosolized delivery of mRNA indicated by luminescence bioactivity. Our interest was specifically in the extent and manner of aerosolization induced particle fusion or aggregation. The cryo-EM results displayed similar size and morphology in the LNPs before aerosolization (denoted as non-aero) for all three samples. Based on previous studies, all three of our samples are lamellar phase LNP-mRNA complexes due to the internal ordering visible within the lipid vesicles.[84–86]

The aerosolized B1 sample without excipients shows considerable susceptibility to the physical stress of nebulization, as visualized in the cryo-EM image (Fig. 9, aero). There is extensive fusion or aggregation present in the B1 sample, causing bleb-like structures over 150 nm in size, as seen previously.[33] Blebbed LNPs resemble a fusion of two or more LNPs which contain a pocket holding mRNA and one or more solvent pockets.[84,87,88] The cryo-EM images of all aerosolized samples indicate that bleb-like structures can form due to aerosolization. The aerosolized B1 image without excipients appears to have lost the lamellar phase pocket containing

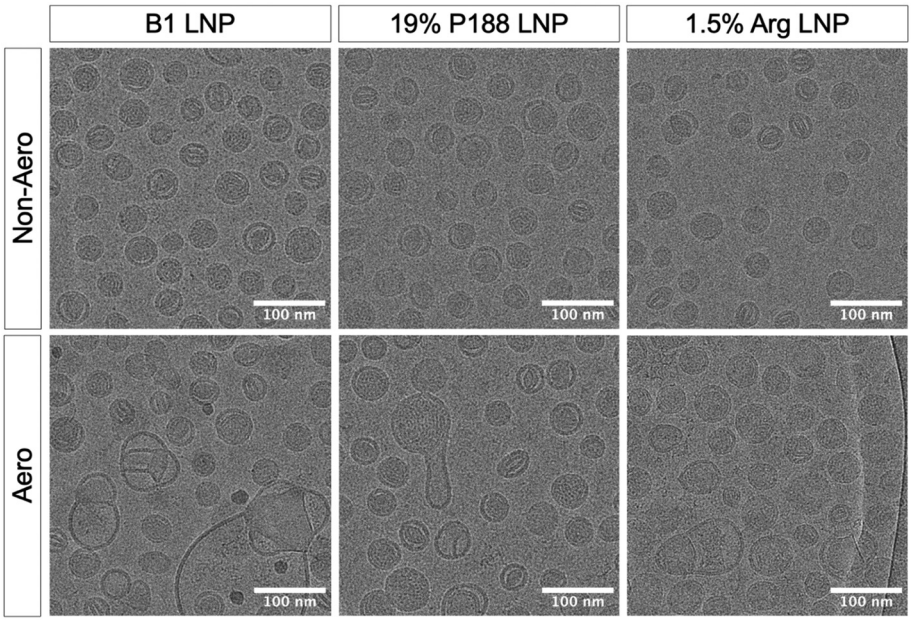

Fig. 9 Cryo-EM images of B1, 19% poloxamer 188, and 1.5% arginine before (Non-Aero) and after (Aero) aerosolization (scale bar = 100 nm).

mRNA in some of the bleb-like structures imaged. Interestingly, images taken from the 19% P188 and 1.5% arginine aerosolized LNPs display the LNPs have fewer overall bleb structures and maintain a lamellar phase structure in the blebbed LNPs that do form. The images from cryo-EM provide strong supporting evidence that poloxamer 188 and L-arginine excipients can better help stabilize the size and structure of LNPs during aerosolization.

3.6 Analyzing LNP structural changes caused by excipients

The internal structure of B1 without excipients and the best performing excipient-doped LNP, 19% P188, were further analyzed using small-angle X-ray scattering (SAXS). Our SAXS profiles of B1 LNP encapsulating NLuc mRNA (denoted as B1_NLuc) and B1 LNP stabilized with 19% P188 (denoted as P188_B1_NLuc) demonstrate that the addition of P188 caused no structural changes to the LNP (Fig. 10). Both profiles are nearly identical, showing no changes in internal structure. A combination of cryo-EM and SAXS indicates that our LNPs have an ordered internal structure likely containing both multilamellar and inverse hexagonal phases of RNA-lipid complexes, similar to those shown in previous studies.[89–91] The sharp Bragg peak centered at q = 0.118 Å^{-1} in both samples correspond to a primary ordered phase with constant 53.1 Å spacing (Fig. 10). However, these peaks are slightly asymmetric due to the coexistence of multiple ordered phases.[92,93] Deconvolution analysis reveals a small secondary ordered phase around q = 0.09 Å, corresponding to constant 68 Å spacing (Fig. S4 and Table S3†). The similarity of the scattering profiles and peak deconvolution analysis for both samples show that excipient incorporation did not cause any noticeable change in the internal LNP structure, and the ordered phase

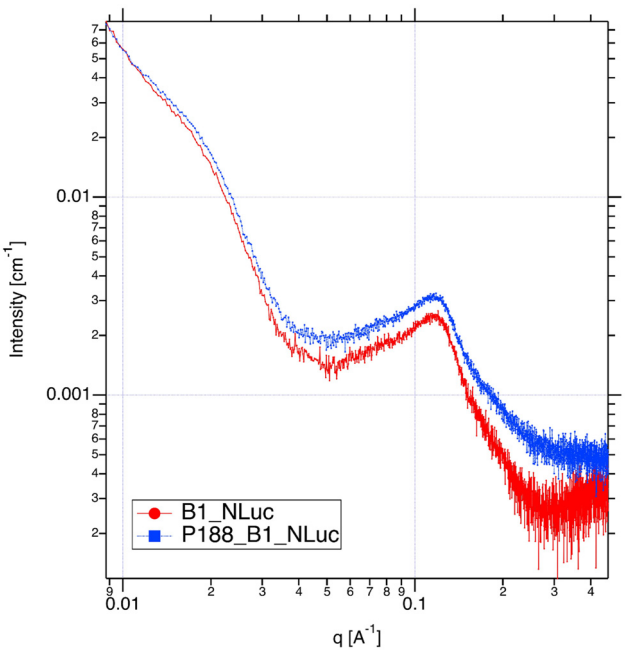

Fig. 10 Synchrotron SAXS profile for B1 (B1_NLuc) and 19% poloxamer 188 (P188_B1_NLuc) LNPs showing no change in the ordered LNP interior with excipient incorporation.

was retained. This indicates that P188 does not incorporate itself within the particle but rather stays on the exterior of the LNP. We hypothesize from this data that P188 likely does not inhibit critical steps in delivery, such as intracellular uptake and endosomal escape, as supported by the luminescent activity.

4. Conclusions

In this study we explored the potential of adding excipients to mRNA LNPs post-formulation to stabilize LNP structures during aerosolization. We utilized a DOE approach to screen twenty-one excipient groups and compared the mRNA expression, size changes, permeability, and LNP morphology before and after aerosolization. Our best performing excipient-doped LNP, with 19% poloxamer 188, displayed superior mRNA expression in lung cells, no significant size changes, and minimal particle-particle fusion as compared to our non-excipient control LNP. While our results indicate that poloxamer 188 does not increase paracellular transport of LNPs, future testing is warranted to understand the mechanism of poloxamer 188 on passive permeability of the cell. Regardless, the success of poloxamer 188 doped mRNA LNP delivery after aerosolization provides a promising avenue for future inhaled LNP therapies to treat pulmonary diseases.

Author contributions

BJH and DG conceptualized and designed experiments. BJH performed most experiments and wrote original manuscript draft. MML supported investigation and methodology. MMZ and AEM performed SAXS analysis of LNPs. EKN and AMH supported experimental investigation. BJH, MML, MMZ, EKN, AMH, AEM, and DG reviewed and edited the manuscript.

Conflicts of interest

BJH and DG have filed a provisional patent on this work. There are no other conflicts of interest.

Data availability

Data for this article, including the raw data for cellular luminescence, LNP size, LNP PDI, LNP encapsulation efficiency, and excipient permeability is available in the Texas Data Repository at **https://dataverse.tdl.org/dataset.xhtml?persistentId=doi:10.18738/T8/FDXMWJ**.

Acknowledgements

The authors would like to thank Dr Axel Brilot and Evan Schwartz for assistance with cryo-EM. Cryo-EM was performed at the University of Texas at Austin Sauer Structural Biology Laboratory (RRID:SCR_022951). The Table of Contents Entry graphic was created in BioRender. Heiser, B. (2025) **https://BioRender.com/i81t870**. Figure 1 was created in BioRender. Heiser, B. (2025) **https://BioRender.com/at6ca6u**.

BJH and DG acknowledge support from Cystic Fibrosis Foundation (GHOSH19XX0).

The SAXS experiments are based on research conducted at the Center for High-Energy X-ray Sciences (CHEXS), which is supported by the National Science Foundation (BIO, ENG and MPS Directorates) under award DMR-2342336, and the Macromolecular Diffraction at CHESS (MacCHESS) facility, which is supported by award 1-P30-GM124166 from the National Institute of General Medical Sciences and the National Institutes of Health.

MMZ and AEM acknowledge support from the University of Texas at Austin and award R35 GM154984 from the National Institute of General Medical Sciences at the National Institutes of Health.

References

1 Y.-S. Wang, M. Kumari, G.-H. Chen, M.-H. Hong, J. P.-Y. Yuan, J.-L. Tsai and H.-C. Wu, *J. Biomed. Sci.*, 2023, **30**, 84.
2 A. Gupta, J. L. Andresen, R. S. Manan and R. Langer, *Adv. Drug Delivery Rev.*, 2021, **178**, 113834.
3 P. S. Kowalski, A. Rudra, L. Miao and D. G. Anderson, *Mol. Ther.*, 2019, **27**, 710–728.
4 C. Wang and H. Liu, *Sci. Rep.*, 2022, **12**, 7259.
5 K. Karikó, H. Muramatsu, F. A. Welsh, J. Ludwig, H. Kato, S. Akira and D. Weissman, *Mol. Ther.*, 2008, **16**, 1833–1840.
6 L. R. Baden, H. M. El Sahly, B. Essink, K. Kotloff, S. Frey, R. Novak, D. Diemert, S. A. Spector, N. Rouphael, C. B. Creech, J. McGettigan, S. Khetan, N. Segall, J. Solis, A. Brosz, C. Fierro, H. Schwartz, K. Neuzil, L. Corey, P. Gilbert, H. Janes, D. Follmann, M. Marovich, J. Mascola, L. Polakowski, J. Ledgerwood, B. S. Graham, H. Bennett, R. Pajon, C. Knightly, B. Leav, W. Deng, H. Zhou, S. Han, M. Ivarsson, J. Miller and T. Zaks, *N. Engl. J. Med.*, 2021, **384**, 403–416.
7 E. J. Anderson, N. G. Rouphael, A. T. Widge, L. A. Jackson, P. C. Roberts, M. Makhene, J. D. Chappell, M. R. Denison, L. J. Stevens, A. J. Pruijssers, A. B. McDermott, B. Flach, B. C. Lin, N. A. Doria-Rose, S. O'Dell, S. D. Schmidt, K. S. Corbett, P. A. Swanson, M. Padilla, K. M. Neuzil, H. Bennett, B. Leav, M. Makowski, J. Albert, K. Cross, V. V. Edara, K. Floyd, M. S. Suthar, D. R. Martinez, R. Baric, W. Buchanan, C. J. Luke, V. K. Phadke, C. A. Rostad, J. E. Ledgerwood, B. S. Graham and J. H. Beigel, *N. Engl. J. Med.*, 2020, **383**, 2427–2438.
8 F. P. Polack, S. J. Thomas, N. Kitchin, J. Absalon, A. Gurtman, S. Lockhart, J. L. Perez, G. P. Marc, E. D. Moreira, C. Zerbini, R. Bailey, K. A. Swanson, S. Roychoudhury, K. Koury, P. Li, W. V. Kalina, D. Cooper, R. W. Frenck, L. L. Hammitt, Ö. Türeci, H. Nell, A. Schaefer, S. Ünal, D. B. Tresnan, S. Mather, P. R. Dormitzer, U. Şahin, K. U. Jansen and W. C. Gruber, *N. Engl. J. Med.*, 2020, **383**, 2603–2615.
9 F. Li, X.-Q. Zhang, W. Ho, M. Tang, Z. Li, L. Bu and X. Xu, *Nat. Commun.*, 2023, **14**, 4223.
10 K. J. Hassett, K. E. Benenato, E. Jacquinet, A. Lee, A. Woods, O. Yuzhakov, S. Himansu, J. Deterling,

B. M. Geilich, T. Ketova, C. Mihai, A. Lynn, I. McFadyen, M. J. Moore, J. J. Senn, M. G. Stanton, Ö. Almarsson, G. Ciaramella and L. A. Brito, *Mol. Ther.-Nucleic Acids*, 2019, **15**, 1–11.

11 L. Miao, L. Li, Y. Huang, D. Delcassian, J. Chahal, J. Han, Y. Shi, K. Sadtler, W. Gao, J. Lin, J. C. Doloff, R. Langer and D. G. Anderson, *Nat. Biotechnol.*, 2019, **37**, 1174–1185.

12 M. M. Billingsley, N. Singh, P. Ravikumar, R. Zhang, C. H. June and M. J. Mitchell, *Nano Lett.*, 2020, **20**, 1578–1589.

13 S. Bevers, S. A. A. Kooijmans, E. Van de Velde, M. J. W. Evers, S. Seghers, J. J. J. M. Gitz-Francois, N. C. H. van Kronenburg, M. H. A. M. Fens, E. Mastrobattista, L. Hassler, H. Sork, T. Lehto, K. E. Ahmed, S. El Andaloussi, K. Fiedler, K. Breckpot, M. Maes, D. Van Hoorick, T. Bastogne, R. M. Schiffelers and S. De Koker, *Mol. Ther.*, 2022, **30**, 3078–3094.

14 J. Li, C. Chen and T. Xia, *Adv. Mater.*, 2022, **34**, e2106456.

15 X. Xu, X. Wang, Y.-P. Liao, L. Luo, T. Xia and A. E. Nel, *ACS Nano*, 2023, **17**, 4942–4957.

16 E. Robinson, K. D. MacDonald, K. Slaughter, M. McKinney, S. Patel, C. Sun and G. Sahay, *Mol. Ther.*, 2018, **26**, 2034–2046.

17 T. Wei, Y. Sun, Q. Cheng, S. Chatterjee, Z. Traylor, L. T. Johnson, M. L. Coquelin, J. Wang, M. J. Torres, X. Lian, X. Wang, Y. Xiao, C. A. Hodges and D. J. Siegwart, *Nat. Commun.*, 2023, **14**, 7322.

18 A. Da Silva Sanchez, K. Paunovska, A. Cristian and J. E. Dahlman, *Hum. Gene Ther.*, 2020, **31**, 940–955.

19 M. R. Soto, M. M. Lewis, J. Leal, Y. Pan, R. P. Mohanty, A. Veyssi, E. Y. Maier, B. J. Heiser and D. Ghosh, *Mol. Ther.-Nucleic Acids*, 2024, **35**(4), 102375.

20 C. J. Woo, A. Allawzi, N. Clark, N. Kaushal, T. Efthymiou, M. Thamsen, J. Nguyen, R. Wooster and J. C. Sullivan, *Pulm. Pharmacol. Ther.*, 2022, **75**, 102134.

21 J. C. Davies, E. W. F. W. Alton and A. Bush, *Br. Med. J.*, 2007, **335**, 1255–1259.

22 Y. Yao and K. Shen, *Pediatr. Invest.*, 2017, **1**, 27–31.

23 Q. Cheng, T. Wei, L. Farbiak, L. T. Johnson, S. A. Dilliard and D. J. Siegwart, *Nat. Nanotechnol.*, 2020, **15**, 313–320.

24 X. Wang, S. Liu, Y. Sun, X. Yu, S. M. Lee, Q. Cheng, T. Wei, J. Gong, J. Robinson, D. Zhang, X. Lian, P. Basak and D. J. Siegwart, *Nat. Protoc.*, 2023, **18**, 265–291.

25 S. A. Dilliard, Q. Cheng and D. J. Siegwart, *Proc. Natl. Acad. Sci. U. S. A.*, 2021, **118**, e2109256118.

26 Q. Li, C. Chan, N. Peterson, R. N. Hanna, A. Alfaro, K. L. Allen, H. Wu, W. F. Dall'Acqua, M. J. Borrok and J. L. Santos, *ACS Chem. Biol.*, 2020, **15**, 830–836.

27 H. Parhiz, V. V. Shuvaev, N. Pardi, M. Khoshnejad, R. Y. Kiseleva, J. S. Brenner, T. Uhler, S. Tuyishime, B. L. Mui, Y. K. Tam, T. D. Madden, M. J. Hope, D. Weissman and V. R. Muzykantov, *J. Controlled Release*, 2018, **291**, 106–115.

28 N. B. Tsui, E. K. Ng and Y. D. Lo, *Clin. Chem.*, 2002, **48**, 1647–1653.

29 C. J. McKinlay, J. R. Vargas, T. R. Blake, J. W. Hardy, M. Kanada, C. H. Contag, P. A. Wender and R. M. Waymouth, *Proc. Natl. Acad. Sci. U. S. A.*, 2017, **114**, E448–E456.

30 B. J. Heiser, A. Veyssi and D. Ghosh, *Nanomedicine*, 2025, **20**, 1043–1069.

31 O. B. Garbuzenko, M. Saad, S. Betigeri, M. Zhang, A. A. Vetcher, V. A. Soldatenkov, D. C. Reimer, V. P. Pozharov and T. Minko, *Pharm. Res.*, 2009, **26**, 382–394.

32 H. Zhang, J. Leal, M. R. Soto, H. D. C. Smyth and D. Ghosh, *Pharmaceutics*, 2020, **12**, 1042.

33 M. M. Lewis, M. R. Soto, E. Y. Maier, S. D. Wulfe, S. Bakheet, H. Obregon and D. Ghosh, *Bioeng. Transl. Med.*, 2023, **8**, e10580.

34 M. P. Lokugamage, D. Vanover, J. Beyersdorf, M. Z. C. Hatit, L. Rotolo, E. S. Echeverri, H. E. Peck, H. Ni, J.-K. Yoon, Y. Kim, P. J. Santangelo and J. E. Dahlman, *Nat. Biomed. Eng.*, 2021, **5**, 1059–1068.

35 S. Liu, Y. Wen, X. Shan, X. Ma, C. Yang, X. Cheng, Y. Zhao, J. Li, S. Mi, H. Huo, W. Li, Z. Jiang, Y. Li, J. Lin, L. Miao and X. Lu, *Nat. Commun.*, 2024, **15**, 9471.

36 J. Kim, A. Jozic, Y. Lin, Y. Eygeris, E. Bloom, X. Tan, C. Acosta, K. D. MacDonald, K. D. Welsher and G. Sahay, *ACS Nano*, 2022, **16**, 14792–14806.

37 H. Miao, K. Huang, Y. Li, R. Li, X. Zhou, J. Shi, Z. Tong, Z. Sun and A. Yu, *Int. J. Pharm.*, 2023, **640**, 123050.

38 X. Hou, T. Zaks, R. Langer and Y. Dong, *Nat. Rev. Mater.*, 2021, **6**, 1078–1094.

39 S. M. Rowe, J. B. Zuckerman, D. Dorgan, J. Lascano, K. McCoy, M. Jain, M. S. Schechter, S. Lommatzsch, V. Indihar, N. Lechtzin, K. McBennett, C. Callison, C. Brown, T. G. Liou, K. D. MacDonald, S. Z. Nasr, S. Bodie, M. Vaughn, E. B. Meltzer and A. J. Barbier, *J. Cyst. Fibros. Off. J. Eur. Cyst. Fibros. Soc.*, 2023, **22**, 656–664.

40 D. E. Geller, C. Crowley, J. Froehlich, C. Schwabe and M. O'Carroll, *J. Cystic Fibrosis*, 2024, **23**, S19.

41 Vertex Announces Investigational New Drug (IND) Application for VX-522, mRNA Therapy for People With Cystic Fibrosis, Cleared by FDA | Vertex Pharmaceuticals, **https://investors.vrtx.com/news-releases/news-release-details/vertex-announces-investigational-new-drug-ind-application-vx-522**, (accessed 11 February 2025).

42 ReCode Therapeutics Announces First Participants Dosed in a Phase 1 Healthy Volunteer Clinical Study of Inhaled mRNA-Based Genetic Medicine, RCT2100, for the Treatment of Cystic Fibrosis, **https://recodetx.com/recode-therapeutics-announces-first-participants-dosed-in-a-phase-1-healthy-volunteer-clinical-study-of-inhaled-mrna-based-genetic-medicine-rct2100-for-the-treatment-of-cystic-fibrosis/**, (accessed 11 February 2025).

43 ReCode Therapeutics Doses First Patient in Phase 1 Clinical Study of Novel mRNA-based Therapy for the Treatment of Primary Ciliary Dyskinesia, **https://recodetx.com/recode-therapeutics-doses-first-patient-in-phase-1-clinical-study-of-novel-mrna-based-therapy-for-the-treatment-of-primary-ciliary-dyskinesia/**, (accessed 12 February 2025).

44 K. J. Kauffman, J. R. Dorkin, J. H. Yang, M. W. Heartlein, F. DeRosa, F. F. Mir, O. S. Fenton and D. G. Anderson, *Nano Lett.*, 2015, **15**, 7300–7306.
45 B. Li, R. S. Manan, S.-Q. Liang, A. Gordon, A. Jiang, A. Varley, G. Gao, R. Langer, W. Xue and D. Anderson, *Nat. Biotechnol.*, 2023, **41**, 1410–1415.
46 M. Massaro, S. Wu, G. Baudo, H. Liu, S. Collum, H. Lee, C. Stigliano, V. Segura-Ibarra, H. Karmouty-Quintana and E. Blanco, *Eur. J. Pharm. Sci.*, 2023, **183**, 106370.
47 X. Bai, Q. Chen, F. Li, Y. Teng, M. Tang, J. Huang, X. Xu and X.-Q. Zhang, *Nat. Commun.*, 2024, **15**, 6844.
48 A. Y. Jiang, J. Witten, I. O. Raji, F. Eweje, C. MacIsaac, S. Meng, F. A. Oladimeji, Y. Hu, R. S. Manan, R. Langer and D. G. Anderson, *Nat. Nanotechnol.*, 2024, **19**, 364–375.
49 C. Yousry, M. Goyal and V. Gupta, *AAPS PharmSciTech*, 2024, **25**, 36.
50 C. A. Schneider, W. S. Rasband and K. W. Eliceiri, *Nat. Methods*, 2012, **9**, 671–675.
51 G. Pilcer and K. Amighi, *Int. J. Pharm.*, 2010, **392**, 1–19.
52 M. Flasiński, M. Gawryś, M. Broniatowski and P. Wydro, *Biochim. Biophys. Acta, Biomembr.*, 2016, **1858**, 836–844.
53 D. Zukancic, E. J. A. Suys, E. H. Pilkington, A. Algarni, H. Al-Wassiti and N. P. Truong, *Pharmaceutics*, 2020, **12**, 1068.
54 T. Arakawa, K. Tsumoto, Y. Kita, B. Chang and D. Ejima, *Amino Acids*, 2007, **33**, 587–605.
55 P. Patel, J. Fetse, C.-Y. Lin, Y. Guo, M. R. Hasan, M. Nakhjiri, Z. Zhao, A. Jain and K. Cheng, *Acta Biomater.*, 2022, **154**, 374–384.
56 T. Ishigami, K. Suga and H. Umakoshi, *ACS Appl. Mater. Interfaces*, 2015, **7**, 21065–21072.
57 Z. Urbán-Morlán, R. Castro-Ríos, A. Chávez-Montes, L. M. Melgoza-Contreras, E. Piñón-Segundo, A. Ganem-Quintanar and D. Quintanar-Guerrero, *J. Pharm. Biomed. Anal.*, 2008, **46**, 799–803.
58 J. G. Moloughney and N. Weisleder, *Recent Pat. Biotechnol.*, 2012, **6**, 200–211.
59 E. van Belle, L. Maillard, A. Rivard, J.-E. Fabre, T. Couffinhal, M. Kearney, D. Branellec, L. J. Feldman, K. Walsh and J. M. Isner, *Hum. Gene Ther.*, 1998, **9**, 1013–1024.
60 D. M. Klein, A. Poortinga, F. M. Verhoeven, D. Bonn, S. Bonnet and C. J. M. van Rijn, *Chem. Phys.*, 2021, **547**, 111192.
61 J. Rodriguez-Loya, M. Lerma and J. L. Gardea-Torresdey, *Micromachines*, 2023, **15**, 24.
62 M. Beck-Broichsitter, M.-C. Knuedeler, N. Oesterheld, W. Seeger and T. Schmehl, *Int. J. Pharm.*, 2014, **459**, 23–29.
63 T. Nguyen, Z. Sosic and C.-F. Xu, *Sep. Sci. plus*, 2024, **7**, e202400045.
64 K. J. Hassett, J. Higgins, A. Woods, B. Levy, Y. Xia, C. J. Hsiao, E. Acosta, Ö. Almarsson, M. J. Moore and L. A. Brito, *J. Controlled Release*, 2021, **335**, 237–246.
65 C. McMillan, A. Druschitz, S. Rumbelow, A. Borah, B. Binici, Z. Rattray and Y. Perrie, *RSC Pharm.*, 2024, **1**, 841–853.
66 T. A. Kwiatkowski, A. L. Rose, R. Jung, A. Capati, D. Hallak, R. Yan and N. Weisleder, *Am. J. Physiol.*, 2020, **318**, C253–C262.
67 I. D. L. Souza, V. Saez and C. R. E. Mansur, *Colloids Surf., B*, 2023, **230**, 113491.
68 N. Hasim, M. A. A. Bakar and M. A. Islam, *Children*, 2021, **8**, 785.
69 P. Barski, M. Surdacki, A. Saj, A. Wróblewska, M. Ornat, A. Pawelak, D. Pompa, J. Jurgiel, V. Ermisch, A. Hirnle, I. Pirogowicz, I. Stanisławska, M. Łyp and M. Pokorski, *Physiol. Res.*, 2020, **69**, S131–S137.
70 T. W. Chin and E. Nussbaum, *J. Pediatr.*, 1992, **120**, 641–643.
71 M. R. Elkins and P. T. Bye, *J. R. Soc. Med.*, 2011, **104**, S2–S5.
72 M. P. Hall, J. Unch, B. F. Binkowski, M. P. Valley, B. L. Butler, M. G. Wood, P. Otto, K. Zimmerman, G. Vidugiris, T. Machleidt, M. B. Robers, H. A. Benink, C. T. Eggers, M. R. Slater, P. L. Meisenheimer, D. H. Klaubert, F. Fan, L. P. Encell and K. V. Wood, *ACS Chem. Biol.*, 2012, **7**, 1848–1857.
73 C. I. Grainger, L. L. Greenwell, D. J. Lockley, G. P. Martin and B. Forbes, *Pharm. Res.*, 2006, **23**, 1482–1490.
74 S. M. Fischer, M. Brandl and G. Fricker, *Eur. J. Pharm. Biopharm.*, 2011, **79**, 416–422.
75 C. De Stefani, J. Lodovichi, L. Albonetti, M. C. Salvatici, J. C. Quintela, A. R. Bilia and M. C. Bergonzi, *Molecules*, 2022, **27**, 3042.
76 T. Kojarunchitt, S. Hook, S. Rizwan, T. Rades and S. Baldursdottir, *Int. J. Pharm.*, 2011, **408**, 20–26.
77 K. A. Min, G. R. Rosania and M. C. Shin, *Cell Biochem. Biophys.*, 2016, **74**, 191–203.
78 Barrier Formation and Permeability Assays using Millicell® Hanging Cell Culture Inserts, **https://www.sigmaaldrich.com/US/en/technical-documents/technical-article/cell-culture-and-cell-culture-analysis/cell-based-assays/barrier-formation-permeability-assays?srsltid=AfmBOoqquEwOgzijdcQNurFvbgsOj7WiI1EAdYNwS_RUuplZbF8KvcYr**, (accessed 13 May 2025).
79 L. Dresser, S. P. Graham, L. M. Miller, C. Schaefer, D. Conteduca, S. Johnson, M. C. Leake and S. D. Quinn, *J. Phys. Chem. Lett.*, 2022, **13**, 5341–5350.
80 H. D. Herce, A. E. Garcia, J. Litt, R. S. Kane, P. Martin, N. Enrique, A. Rebolledo and V. Milesi, *Biophys. J.*, 2009, **97**, 1917–1925.
81 C. Allolio, A. Magarkar, P. Jurkiewicz, K. Baxová, M. Javanainen, P. E. Mason, R. Šachl, M. Cebecauer, M. Hof, D. Horinek, V. Heinz, R. Rachel, C. M. Ziegler, A. Schröfel and P. Jungwirth, *Proc. Natl. Acad. Sci. U. S. A.*, 2018, **115**, 11923–11928.
82 S. F. Verbeek, N. Awasthi, N. K. Teiwes, I. Mey, J. S. Hub and A. Janshoff, *Eur. Biophys. J.*, 2021, **50**, 127–142.
83 F. Lindenberg, F. Sichel, M. Lechevrel, R. Respaud and G. Saint-Lorant, *J. Toxicol. Risk Assess.*, 2019, **5**, 022.
84 M. L. Brader, S. J. Williams, J. M. Banks, W. H. Hui, Z. H. Zhou and L. Jin, *Biophys. J.*, 2021, **120**, 2766–2770.

85 L. Zheng, S. R. Bandara, Z. Tan and C. Leal, *Proc. Natl. Acad. Sci. U. S. A.*, 2023, **120**, e2301067120.
86 R. Pattipeiluhu, Y. Zeng, M. M. R. M. Hendrix, I. K. Voets, A. Kros and T. H. Sharp, *Nat. Commun.*, 2024, **15**, 1303.
87 A. K. K. Leung, Y. Y. C. Tam, S. Chen, I. M. Hafez and P. R. Cullis, *J. Phys. Chem. B*, 2015, **119**, 8698–8706.
88 M. H. Y. Cheng, J. Leung, Y. Zhang, C. Strong, G. Basha, A. Momeni, Y. Chen, E. Jan, A. Abdolahzadeh, X. Wang, J. A. Kulkarni, D. Witzigmann and P. R. Cullis, *Adv. Mater.*, 2023, **35**, 2303370.
89 J. A. Kulkarni, M. M. Darjuan, J. E. Mercer, S. Chen, R. Van Der Meel, J. L. Thewalt, Y. Y. C. Tam and P. R. Cullis, *ACS Nano*, 2018, **12**, 4787–4795.
90 M. Farzan, A. Ross, C. Müller and A. Allmendinger, *Eur. J. Pharm. Biopharm.*, 2022, **181**, 270–281.
91 H. M. Dao, K. AboulFotouh, A. F. Hussain, A. E. Marras, K. P. Johnston, Z. Cui and R. O. Williams, *Pharm. Res.*, 2024, **41**, 501–512.
92 M. Hammel, Y. Fan, A. Sarode, A. E. Byrnes, N. Zang, P. Kou, K. Nagapudi, D. Leung, C. C. Hoogenraad, T. Chen, C.-W. Yen and G. L. Hura, *ACS Nano*, 2023, **17**, 11454–11465.
93 M. Yanez Arteta, T. Kjellman, S. Bartesaghi, S. Wallin, X. Wu, A. J. Kvist, A. Dabkowska, N. Székely, A. Radulescu, J. Bergenholtz and L. Lindfors, *Proc. Natl. Acad. Sci. U. S. A.*, 2018, **115**, E3351–E3360.